https://doi.org/10.5194/egusphere-2026-1924
Preprint. Discussion started: 14 April 2026

A different take on fission-track annealing in apatite

Raymond Jonckheere[a]*, Florian Trilsch[a], Birk Härtel[b], and Thorsten Nagel[a]

[a]Endogene Geologie, Geologisches Institut, Technische Universität Bergakademie Freiberg, Bernhard-von-Cotta-Straße 2, 09599 Freiberg, Germany

[b]Department of Earth, Energy, and Environment, University of Calgary, 2500 University Drive NW, Calgary, AB, Canada, T2N 1N4

(Raymond.Jonckheere@geo.tu-freiberg.de; Florian.Trilsch@geo.tu-freiberg.de; Birk.Haertel@ucalgary.ca; Thorsten.Nagel@geo.tu-freiberg.de)

Abstract

This work discusses a model for calculating the mean-lengths of confined fission tracks in apatite after isothermal heating. We derive separate equations for gradual and accelerated high-temperature annealing, and for ambient-temperature annealing. A three-parameter fanning Arrhenius model describes the initial gradual length reduction in all apatites. A linear equation corrects for the different rates of length reduction in different apatite compositions during subsequent accelerated annealing. Another linear equation describes ambient-temperature annealing at lab and geological timescales. At present, these equations give the mean track length in the most and least resistant apatites over their full annealing ranges, at all time-temperature conditions. The aim is not to achieve greater precision or accurateness than existing equations. Instead, we made some choices and concessions in order to combine different datasets, and construct an annealing model that aims to be a reasonable approximation across different apatites and measurement protocols. The calculated age-vs.-depth profile for the Kontinentale Tiefbohrung fits the data almost without compromise for a cooling path constrained by independent geological and thermochronological evidence. In contrast, the mean-length-vs.-depth profile is offset to higher values than the length data. Experimental factors and ambient-temperature annealing could in part be responsible. The inconclusive fit to geological data emphasizes the need for a consensus on a set of reliable geological benchmarks.

Keywords

Fission track; annealing model; confined-track length; apatite composition; measurement bias; geological benchmark.

* Corresponding author

https://doi.org/10.5194/egusphere-2026-1924
Preprint. Discussion started: 14 April 2026

1. Introduction

Fission tracks in apatite shorten and fade through a range of temperatures relevant to geological processes such as basin subsidence and uplift, erosional and tectonic unroofing, thrust tectonics, and hydrocarbon maturation. A quantitative understanding of track shortening is fundamental to interpreting fission-track ages and modelling geological thermal histories. To that end, investigators have undertaken comprehensive experiments, in which confined track lengths and orientations were measured in samples with induced tracks, held at fixed temperatures for different durations (Green et al., 1986; Crowley et al., 1991; Carlson et al., 1999; Barbarand et al., 2003; Ravenhurst et al., 2003; Tello et al., 2006; Tamer and Ketcham, 2020). Equations were fitted to the data, most assuming dependence on reciprocal temperature, T^{-1}, and the logarithm of annealing time, ln(t), resulting in straight or curved, parallel or fanning, iso-retention lines in an Arrhenius diagram. Wauschkuhn et al. (2015; their Table 6) list 24 models for apatite, and more can be found in the literature. The annealing equations were complemented with additional equations, e.g., relating the standard deviation of the length distribution to the mean, and the surface track density to the mean track length. Table 5 of Wauschkuhn et al. (2015) provides a sample of these equations.

The annealing experiments revealed that track shortening in apatite is anisotropic and proceeds in stages: an initial gradual stage and a later stage of accelerated shortening, first affecting tracks at high angles to the ***c***-axis, and extending to lower angles with progressive annealing. Green et al. (1986) attributed the latter stage in part to track break-up, in contrast to Donelick (1991), who referred to it as accelerated annealing. Donelick et al. (1999) and Ketcham et al. (2007) proposed converting each measured length to the corresponding length of a track parallel to the ***c***-axis (***c***-axis projection). This eliminates length anisotropy and, at the same time, the distinction between gradual and accelerated annealing. The resulting view of annealing is somewhat similar to continuous shortening under an external load, with each apatite composition characterized by its specific resistance.

It remains uncertain how well these elements combine to predict accurate ages and length distributions for given thermal histories. The fact that track counts (Jonckheere and Van den haute, 1998; 1999; 2002; Aslanian et al., 2022) and mean track lengths (Barbarand et al., 2003; Ketcham et al., 2009; 2015; Tamer et al., 2019) are often not reproducible within statistical error raises concern about the appropriateness of empirical equations under different conditions and for other analysts and samples. In this work, we focus on predicting the age and mean track length rather than the length distribution, which is more sensitive to deviations from the model equations. We accept that etching, selection and measurement of confined tracks contribute to mean-length discrepancies (Aslanian et al., 2021; Trilsch et al. 2023; Fu et al., 2024), and therefore tolerate minor statistical inconsistencies, seeking instead an equation that is a fair approximation for different experimental conditions. This allows us to integrate the main multi-compositional sets of measurements of confined tracks in apatite prism faces, etched in concentrated nitric-acid (Carlson et al., 1999; Barbarand et al., 2003; Ravenhurst et al., 2003; Tamer and Ketcham, 2020). Limiting our calculations to the mean track length removes the need to consider angular data and the consequences of ***c***-axis projection, while retaining a meaningful measure of the aggregate annealing effect. It does not, however, eliminate the distinction between gradual and accelerated annealing. It also does not permit us to ignore differences between apatites due to their chemical compositions.

Figure 1 illustrates our approach; it plots the mean track length, L, vs. *Dpar* for fifteen apatites included in three annealing runs (Carlson et al., 1999); the solid line is a fit to the unannealed samples. At the first annealing stage, nine samples plot on a parallel line, while six plot just below

https://doi.org/10.5194/egusphere-2026-1924
Preprint. Discussion started: 14 April 2026

it. At the second stage, six samples plot on a parallel line while nine plot ~1.0 - 5.0 µm below it. We observe that Figure 1 illustrates the *differences* between samples, not the consequences of annealing as such. Corresponding plots for the complete datasets of Carlson et al. (1999), Barbarand et al. (2003), and Ravenhurst et al. (2003) show the same trend (Supplement Figure S1), characterized by an initial gradual stage, during which all mean lengths shorten at the same rate, and an accelerated stage, during which the mean track length in a growing subset of the samples breaks down. These observations suggest that the induced tracks in different apatites do not anneal at different *overall* rates, but experience accelerated shortening at different points along their annealing trajectories, i.e., at different mean lengths. We therefore distinguish the annealing trajectories of different apatites based on a failure threshold (L_{acc}) rather than a rate coefficient (r_{mr0}; Ketcham et al., 1999). This has some support from the relationship between the reduced mean lengths and normalized densities of induced tracks in different apatites (Green, 1988; Guedes et al., 2004). The break-in-slope, which marks the approximate onset of accelerated annealing, occurs later in Durango apatite than in Renfrew fluorapatite, and later still in the Strontian apatite (Supplement Figure S2). The annealing data for the Tioga apatite (Donelick, 1991) and Durango apatite (Donelick et al., 1999) also suggest that the former has a higher threshold for accelerated annealing.

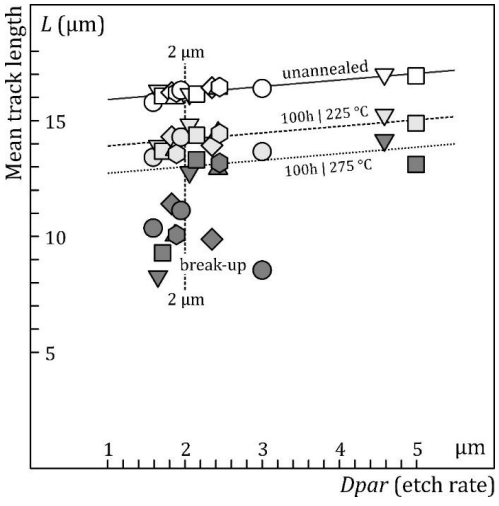

Figure 1. Mean lengths, *L*, of induced confined tracks in different apatites at progressive annealing stages, plotted against *Dpar*; the unannealed tracks plot about a linear trend (no shading, solid line); the onset of accelerated shortening causes a set of six samples with 1.5 µm < Dpar < 3 µm to inch ahead of a line of constant length reduction (light shading; dashed line); further annealing causes nine samples to separate from a line of constant length reduction (dark shading; dotted line). Data from Carlson et al. (1999; 20 s in 5.5 M HNO_3 at 21 °C).

This leads us (1) to separate the initial gradual and subsequent accelerated annealing stages of individual samples, (2) to fit one annealing equation to the common gradual stage of the samples, and (3) to account for compositional differences during the accelerated stage. We calculate age- and mean-length profiles for the *Kontinentale Tiefbohrung* to assess the performance of our model, and discuss methodological issues arising from comparing its predictions with geological benchmarks.

2. Annealing model

The above implies that the initial gradual annealing of all apatite compositions can be described with one equation if we measure the mean-length reduction as $S = L_0 - L$ (Carlson, 1990; L_0: unannealed mean length; L: annealed mean length) instead of $r = L/L_0$ (Green et al., 1985). We used the multi-compositional high-temperature data of Carlson et al. (1999), Barbarand et al. (2003), and Ravenhurst et al. (2003), comprising measurements of induced tracks in apatite prism faces,

https://doi.org/10.5194/egusphere-2026-1924
Preprint. Discussion started: 14 April 2026

etched with similar high HNO_3-concentrations (5.0-5.5 M). In the case of Barbarand et al. (2003), we averaged the results of different experimenters for each annealing run. Measurements considered to reveal accelerated shortening were excluded from fitting the gradual stage on the basis of Supplement Figure S1. We first fitted each isochronal experiment, assuming that S (µm) correlates with the reciprocal temperature (1000 T^{-1} (K^{-1}); Green et al., 1985; Laslett et al., 1987; Crowley et al., 1991; Ketcham et al., 1999; 2007). Supplement Figure S3 shows the fits to the data of Carlson et al. (1999), Barbarand et al. (2003) and Ravenhurst et al. (2003). The fitted equation has the form:

$$S = A_1 + \frac{B_1}{\frac{1000}{T} - C_1} \quad (1)$$

Herein, S (= L_0 - L) is the mean-length reduction, and A_1, B_1, and C_1 are fitted model parameters. A_1 (µm) shifts the model curve along the S-axis, B_1 (µm/K) stretches is along the same axis, and C_1 (K^{-1}) shifts the model along the temperature axis. In simple, approximate terms, $|A_1| + L_0$ (unannealed mean length) can be thought of as the "zero-length", the mean length of tracks held for some length of time at absolute zero temperature (T_0 = 0 K). Given that L_0 is the reference length for calculating S, we should expect that $A_1 \leqslant 0$. C_1 can be considered as related to the temperature of instantaneous annealing (T_∞; $C_1 = 1000/T_\infty$). The fitted values of A_1, B_1, and C_1 are listed in Supplement Table T1, together with the correlation coefficients and the mean squared deviations of the fits.

Figure 2 shows A_1 (2a), B_1 (2b), and C_1 (2c) plotted against the duration, $\ln(t)$, of each isochronal experiment. The fact that the trends of A_1 vs. $\ln(t)$ and B_1 vs. $\ln(t)$ are erratic, as well as the clear anti-correlation between A_1 and B_1 (2d), suggests that - simple as it is - this model is still overparametrized. We therefore settled on a model with just two parameters, A_2 and B_2, that is also a good fit. Supplement Table T1 lists their values, with correlation coefficients and mean squared residuals.

$$S = A_2 + \frac{B_2}{\frac{1000}{T} - B_2} \ (\times\ 1\ \mu m) \quad (2)$$

This model is somewhat inelegant in terms of the units of A_2 (µm) and B_2 (K^{-1}), requiring a correction (×1 µm) to give S in µm; however, both parameters exhibit a linear correlation with $\ln(t)$ (Figure 2e-f).

$$A_2 = U_A \ln(t) + V_A \quad (3)$$

$$B_2 = U_B \ln(t) + V_B \quad (4)$$

Supplement Table T2 summarizes the parameters of the regression lines in Figure 2e and f, as well as independent U_A, V_A, U_B, and V_B-estimates obtained by direct fitting of equations (2)-(4) to the measured mean track lengths. In both cases (A_2 and B_2), the response surfaces have long flat-bottomed troughs, within which (U_A, V_A) and (U_B, V_B) provide a more or less tolerable fit (Figure 3). These are an expression of the limited wobble of the regression lines about the centroids of the data in Figures 2e and f. The final parameter estimates based on regression and on the mean squared residuals are nevertheless close. In both cases U_A is close to zero. Insofar that it represents the unannealed track length ($|A_2| + L_0$), one would indeed expect that A_2 is independent of the annealing time, $\ln(t)$. Refitting with the constraint that U_A = 0 has but a minor effect on the other parameters, and on the whole, the different estimates are in agreement (Supplement Table T2 and Figure 3).

https://doi.org/10.5194/egusphere-2026-1924
Preprint. Discussion started: 14 April 2026

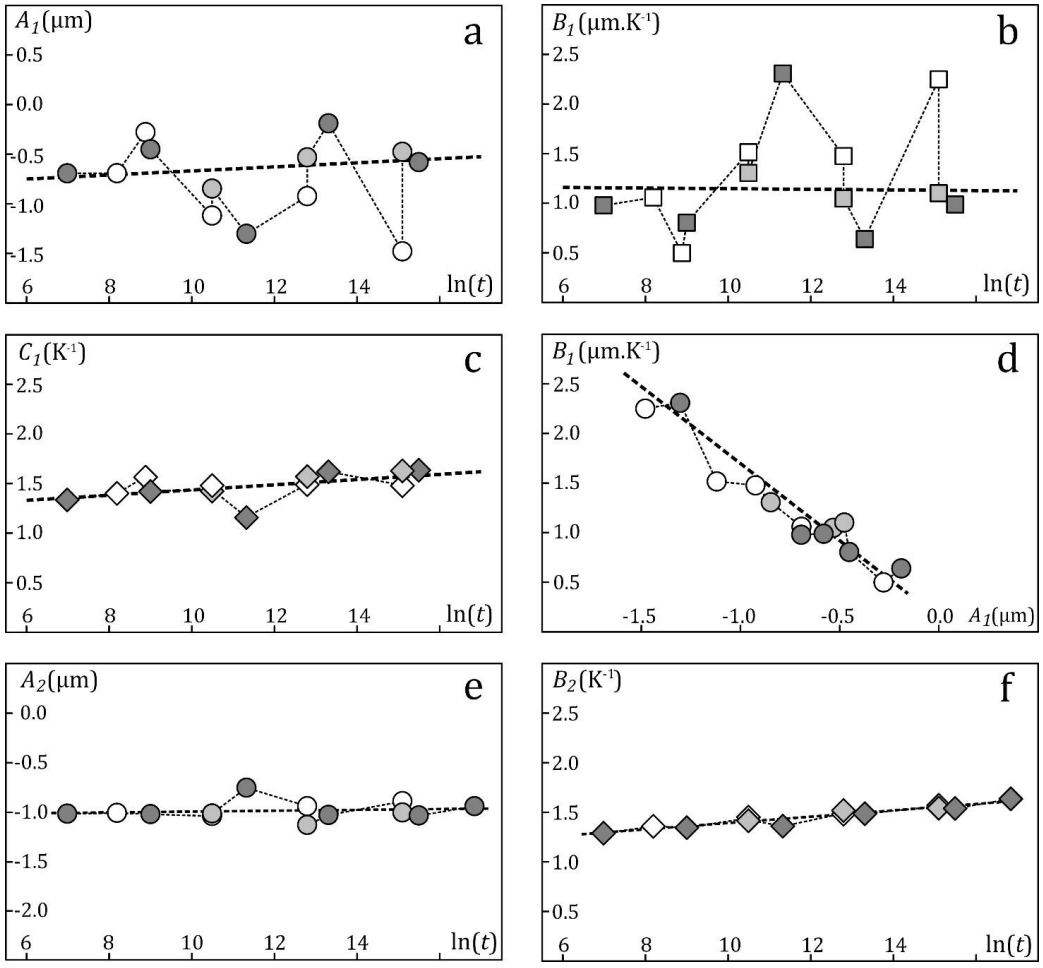

Figure 2. Isochronal annealing experiments: model-1 (A_1, B_1, C_1; equation 1) and model-2 (A_2, B_2; equation 2) parameters plotted against annealing time: **(a)** A_1 vs. ln(t); **(b)** B_1 vs. ln(t); **(c)** C_1 vs. ln(t); **(d)** B_1 vs. A_1; **(e)** A_2 vs. ln(t); **(f)** B_2 vs. ln(t). Open symbols: parameters of the equations fitted to the data of Carlson et al. (1999); light shading: to the data of Barbarand et al. (2003); dark shading: to the data of Ravenhurst et al. (2003).

Figure 4 presents the residual-distributions for the final model (U_A = 0). The Carlson et al. (1999) data have an excess of negative values (median -0.058 µm), as also the Barbarand et al. (2003) data (median -0.038 µm), while the Ravenhurst et al. (2003) data have an excess of positive residuals (median +0.107 µm). Positive residuals mean that the measured track lengths are longer than predicted. The combined data have a small excess of negative values (median -0.025 µm). A normal distribution fitted to the data has a correlation coefficient of 0.982, and mean and standard deviation of -0.029 µm and 0.222 µm. These differences mean that the data are not consistent with each other. We believe that the likeliest causes are the different etching, selection and measurement protocols, rather than sample preparation, temperature control or the annealing duration. Excluding one or two datasets would in effect come down to a bias against the deselected, and in favour of the remaining data, and result in an equation valid for that specific selection. We therefore prefer to proceed with all the data and to accept the loss of resolution that comes with it. Our annealing model will in consequence be less accurate and precise for each individual set of measurements, but more robust overall, including some other protocols used in geological investigations.

https://doi.org/10.5194/egusphere-2026-1924
Preprint. Discussion started: 14 April 2026

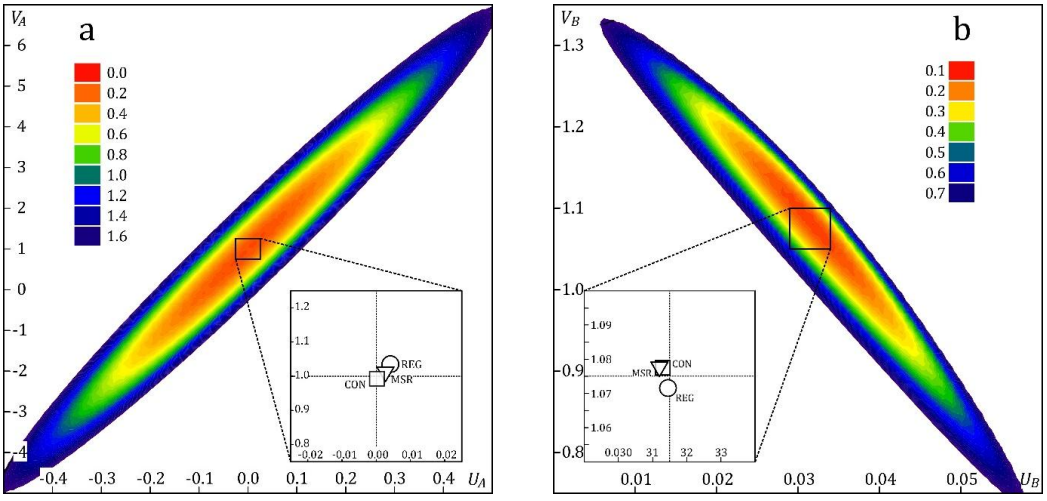

Figure 3. (a) Parameter estimates (U_A, V_A) of equation (3) for the combined data; REG: based on regression (Figure 2e); MSR: based on residuals; CON: with constraint U_A = 0. **(b)** parameter estimates (U_B, V_B) of equation (4); REG: based on regression (Figure 2f); MSR: based on residuals; CON: with constraint U_A = 0 (Supplement Table T2).

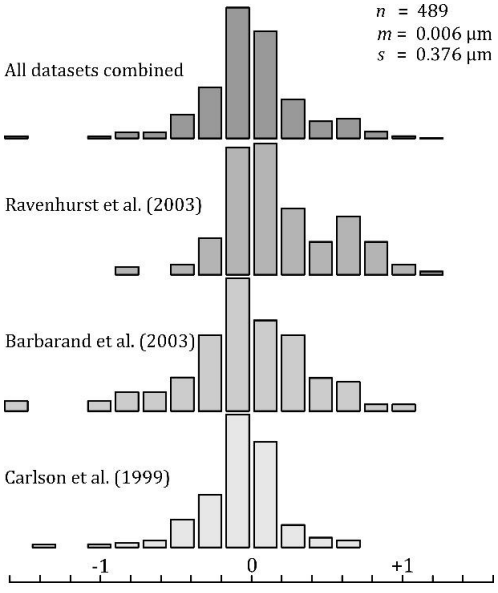

Figure 4. Residuals; very light shading: Carlson et al. (1999); light shading: Barbarand et al. (2003); medium: Ravenhurst et al. (2003); dark: combined data; *n*: number of experiments; *m*: mean; *s*: standard deviation.

3. Apatite composition

Equations (2)-(4) give the mean-length reduction of confined tracks that undergo no accelerated annealing down to ~8 µm. Less resistant apatites require a correction factor related to the sample composition. Ketcham et al. (1999) determined kinetic parameters (r_{mr0}, κ) from apatite-to-apatite matching, and correlated them with *Dpar* and the anion site occupation; later studies included other factors. Supplement Figure S1 suggests that the annealing trajectories in different apatites could be more a matter of the point where accelerated shortening sets than of their overall rates of shortening. This also requires an additional kinetic parameter that can be estimated by apatite-to-apatite matching. Figure 5 plots the length shortening in Renfrew fluorapatite (RN; S_F) against

https://doi.org/10.5194/egusphere-2026-1924
Preprint. Discussion started: 14 April 2026

that in Bamble (B3; S_B) under identical annealing conditions (data from Carlson et al., 1999). Bamble is the most resistant apatite and Renfrew the least (Ketcham et al., 1999). As most data constraining our model at high degrees of annealing are Bamble data, or consistent with them (Supplement Figure S1), we assume that the abscissa in Figure 5 corresponds to the model equations (2)-(4).

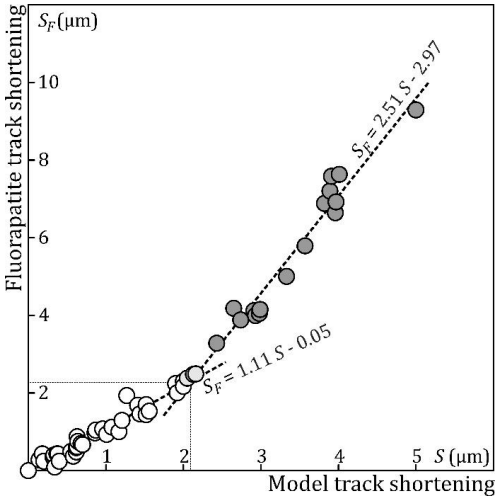

Figure 5. Empirical relationship between the average shortening of fission tracks in a fluorapatite (S_F) and in a reference apatite, which does not undergo accelerated length reduction (S_B). Data from Carlson et al. (1999).

We fitted the data in Figure 5 by two linear sections, intersecting at $S_F \approx 2.1$ μm (Supplement Table 3). The section up to 2.1 μm is associated with initial gradual shortening at the same rate for RN and B3. From 2.1 μm, accelerated annealing sets in in RN, causing 2.51× faster shortening (R_F = 2.51) in Renfrew than calculated with equations (2)-(4) for the most resistant Bamble apatite. We use this relationship for calculating the track lengths in fluorapatite. Similar estimates can be obtained for other compositions, e.g., we calculated for Durango that $S_D \approx 3.2$ μm and $R_D \approx 2.56$. This result was however obtained after excluding three conspicuous outliers, and is not considered further.

If other apatites have similar R_D, it would indicate that the fundamental distinction between them is the length at which accelerated annealing begins. It is tempting to relate this to the concepts of latent-tracks as consisting of a cylindrical midsection and conical extensions to either side, and of annealing as a process of radial contraction (Carlson, 1990; Li et al., 2012). This could account for the fact that high-angle tracks with lesser diameters break-up earlier than low-angle tracks with larger diameters (Green et al., 1986; Donelick, 1991; Paul and Fitzgerald, 1992; Paul, 1993). Although the transmission-microscopic studies of Li et al. (2014) disconfirmed orientation dependent track diameters, the SAXS-investigations of Afra et al. (2014) and Nadzri et al. (2016; 2017) reconfirmed them. There is a notable parallel between our two-stage approach to annealing and their description of annealing as a two-step process of radial shrinkage, both with their transitions dependent on composition. This would suggest a close relationship between the latent-track diameter and the onset of accelerated annealing within one apatite and between apatites, reflected in our model.

4. Ambient-temperature

Regardless of composition, equations (2)-(4) with the parameters in Supplement Table T2 imply that, at <25 °C, no shortening occurs in less than a year and ≲1 μm at all geological timescales up

https://doi.org/10.5194/egusphere-2026-1924
Preprint. Discussion started: 14 April 2026

to 1 Ga. This contradicts ambient-temperature experiments and measurements on geological samples with known thermal histories (Gleadow and Duddy, 1981; Donelick et al., 1990; Vrolijk et al., 1992; Spiegel et al. 2007; Wauschkuhn et al., 2015; Tamer and Ketcham, 2020). This could mean that the annealing parameters are inaccurate or that the model equations are unsuitable. On the other hand, it could also point to radiation damage effects (Hendriks and Redfield, 2005; Li et al., 2017; McDannell et al., 2019), or to a competing process (ageing; Gleadow et al., 1983; Durrani and Bull, 1987). If we consider ambient-temperature annealing of induced tracks in the lab and fossil tracks in geological samples as one process, then radiation damage is excluded. If ageing is understood as limited to geological timescales, then it is also excluded, but if it is understood as any time-dependent track shortening different from that in high-temperature lab experiments, then it is not.

Figure 6 plots the short- time, low-temperature annealing data of Tamer and Ketcham (2020) as S vs. ln(t). We excluded older experiments, which did not include measurements of an internal length standard, because biases related to track etching, selection and measurement can have a disproportionate effect, given that the shortening is ≪1 µm in most cases. The samples from previous studies are also sometimes unevenly distributed on the ln(t)-scale. We concede that this decision is prone to potential bias but that applies to any other decision of which measurements to include as well. In three out of four cases (except Durango), regression lines fitted to the data predict 1.5-2.5 µm shortening on a geological timescale, within ≲0.3 µm of the mean fossil track lengths (Supplement Table T3). On this assumption, the lengths of fossil tracks in geological reference samples can be accounted for without having to alter the main equation or adjust the model parameters.

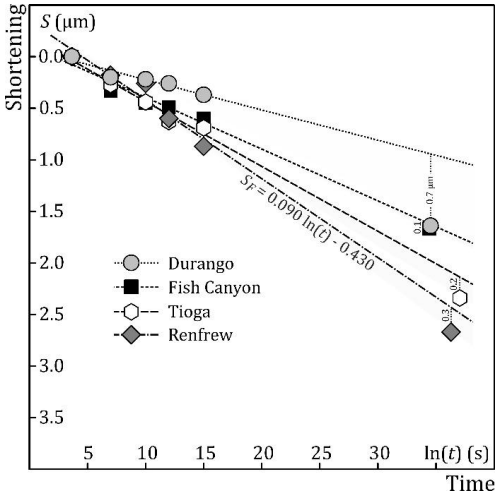

Figure 6. Regression lines fitted to the controlled short-duration ambient-temperature annealing data of Tamer and Ketcham (2020; Table 2, excluding external data). A linear fit to the shortening (S) vs. ln(t) predicts 1.5 - 2.5 µm length reduction at geological timescales, which in three out of four cases (except Durango) are in fair agreement (<0.3 µm difference) with measurements on fossil tracks.

5. Geological timescales

Figure 7 presents Arrhenius plots for an apatite wherein the tracks undergo no accelerated length reduction down to a mean length of ~8 µm (Figure 7a; e.g., Bamble), and for an apatite with minimal resistance to annealing (Figure 7b; e.g., Renfrew; $S_F \approx 2$ µm). Both graphs show fanning straight lines of equal mean length reduction, forming a reasonable connection between lab and geological annealing. The plots are identical between $S = 0$ and 2 µm; the difference is in the spacing of the iso-retention lines for S = 2-8 µm, due to accelerated shortening of the tracks in the less resistant apatite.

https://doi.org/10.5194/egusphere-2026-1924
Preprint. Discussion started: 14 April 2026

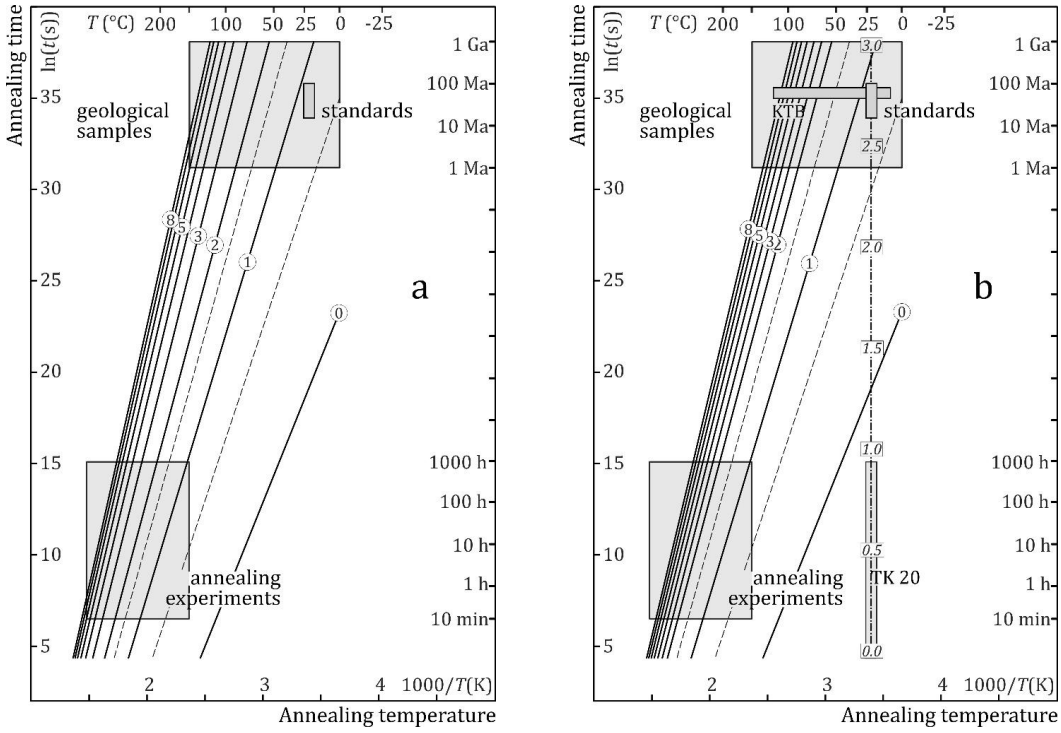

Figure 7. (a) Arrhenius diagram for a reference apatite that experiences no accelerated length reduction; **(b)** Arrhenius diagram for a representative fluorapatite. The numbers in circles give the length reduction in µm estimated from the high-*T* annealing experiments of Carlson et al. (1999), Barbarand et al. (2003) and Ravenhurst et al. (2003). The numbers in boxes give the estimated length reduction in µm based on the low-*T* experiments of Tamer and Ketcham (2020), assuming logarithmic time dependence and no temperature dependence.

The $S = 0$ line excludes shortening at ambient temperatures on lab timescales and limits that on geological timescales to $\lesssim$1 µm, in contrast to the experimental findings cited above (section 4). To fit the low-temperature data one could adjust the model parameters (Guedes et al., 2008) or the equations (Carlson, 1990; Crowley et al., 1991; Ketcham et al., 1999), or consider a separate process (ageing: Gleadow et al., 1983; seasoning: Durrani and Bull, 1987; unspecified: Tamer and Ketcham, 2020). Ageing and seasoning are low-temperature processes on geological timescales, while the latter operates on lab timescales. We do not distinguish between long and short timescales (Figure 6), and propose a solution involving two processes with different kinetics operating throughout. This is conjecture, but it could solve both apparent inconsistencies without affecting the annealing model. As an example of two processes with different kinetics operating in parallel, one could think of the nucleation and growth of crystalline kernels inside an amorphous track core.

To evaluate the model predictions at geological annealing temperatures and timescales, we consider the Kontinentale Tiefbohrung (KTB) on the western margin of the Bohemian Massif. The samples' *Tt*-histories and fission-track properties are the product of Late Cretaceous to Palaeocene exhumation and cooling and subsequent holding at near-constant temperatures. Wauschkuhn et al. (2015) reviewed the geological and thermochronological evidence. Wagner et al. (1994), Coyle et al. (1997) and Wauschkuhn et al. (2015) reported age- and length-vs.-depth data.

https://doi.org/10.5194/egusphere-2026-1924
Preprint. Discussion started: 14 April 2026

Figure 8 plots the low-temperature thermochronometric ages of near-surface samples from the Kontinentale Tiefbohrung against their closure temperatures. The assumed *Tt*-path of a surface sample begins before 85 Ma, at 170 °C, i.e., within the total annealing zone of the most resistant apatite. It cooled for 32 Ma at 5°C/Ma and thereafter remained at 10°C; deeper samples had parallel *Tt*-histories, offset by 10°C. We used the present surface temperature and geothermal gradient (7.5°C + 27.5 °C/km; Clauser et al., 1997) for converting the temperatures to depths. We applied equations (2)-(4) and, for comparison, the parameters for the most and least resistant apatites for calculating *S*. Supplement Table T4 lists the equations for the initial mean length (L_0; Carlson et al., 1999), the standard deviation (Donelick et al., 1999), and the relationship between the reduced track densities and normalized mean lengths. The latter was not taken from earlier work but is based on the observation that accelerated annealing in the least resistant apatite begins at $S \approx 2.1$ µm, and the fact that annealing is complete at $L/L_0 \approx 0.5$. Although it is a core element of *Tt*-modelling, this relationship is one of the least certain and least constrained by data. Most published equations do not distinguish between compositional varieties, and there is little agreement among them (Supplement Figure S4). The preferred equation is consistent with our assumption that the core difference between apatite varieties lies in the onset of accelerated shortening and segmentation. Our calculations used a 0.1-Ma time step and applied the principle of equivalent time.

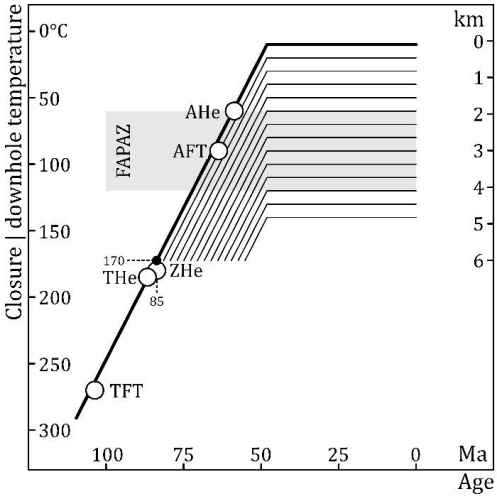

Figure 8. Proposed cooling paths of samples from the Kontinentale Tiefbohrung during their Late-Cretaceous to Palaeocene exhumation. TFT: representative titanite fission-track age of samples below the fossil partial annealing zone (Coyle and Wagner, 1998); THe: titanite He-age of near-surface samples (Stockli and Farley, 2004); ZHe: zircon He-age of near-surface samples (Wolfe and Stockli, 2010); AFT: apatite fission-track age of near-surface samples (Wagner et al., 1994); AHe: apatite He-age of near-surface samples (Warnock et al., 1997).

Figure 9 shows the age- (9a) and length-vs.-depth (9b) profiles. The dashed lines refer to the most resistant apatite and the solid lines to the least resistant; the dot-dash line is a linear extrapolation of the data of Tamer and Ketcham (2020) to geological holding times (Figures 6 and 7b). The fit to the age data of Wagner et al. (1994) is surprising for a simple three-parameter fanning Arrhenius model, fitted to different annealing datasets without great concern for their statistics. The compositional correction appears to be consistent with the negligible Cl-content of the KTB apatites over the entire height of the profile, whereas the elevated OH-concentrations would suggest a much greater resistance. This means that either the calculated OH-concentrations are not reliable or that OH is not the best kinetic indicator (Ketcham et al., 1999; 2007; Wauschkuhn et al., 2015). Given its derivation, it is not unreasonable to assume that the good fit is in some part fortuitous.

https://doi.org/10.5194/egusphere-2026-1924
Preprint. Discussion started: 14 April 2026

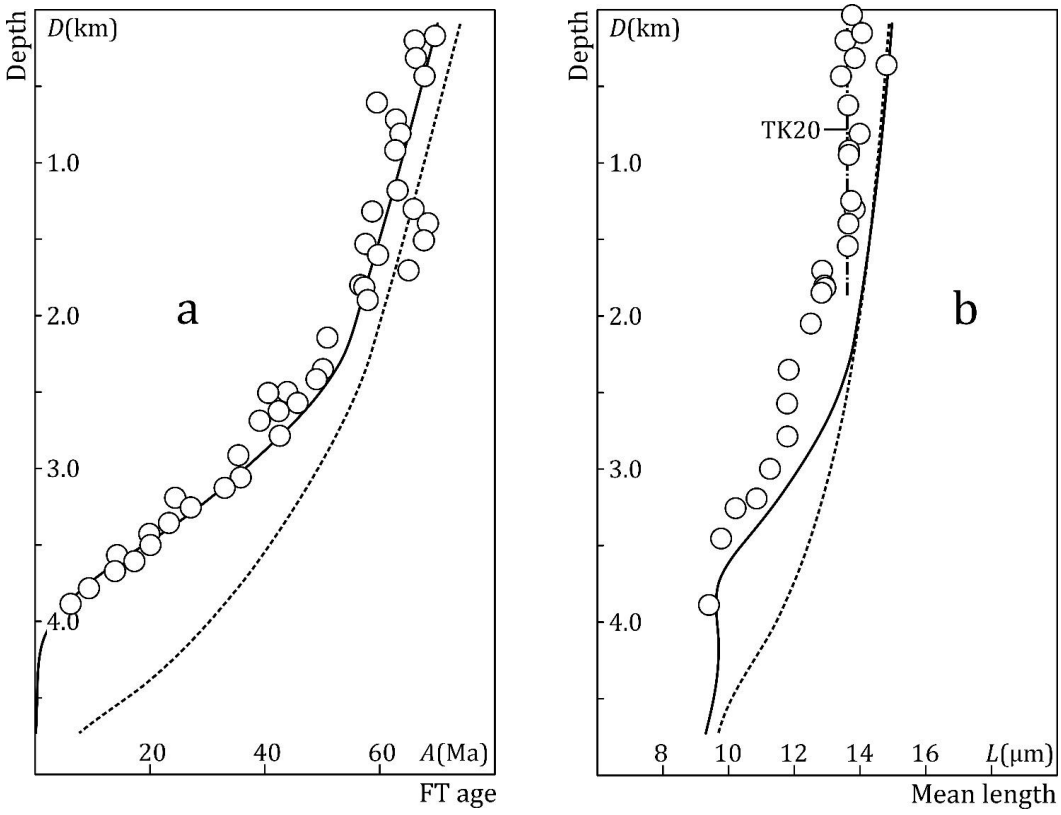

Figure 9. (a) Fission-track age vs. depth profiles calculated with model-2; (**b**) mean confined track length vs. depth profiles. Dashed lines refer to an apatite that undergoes no accelerated length reduction; the solid lines refer to a representative fluorapatite; the dash-dot line assumes low-*T* annealing independent of sample depth (<50 °C), based on our interpretation of the data of Tamer and Ketcham (2020). Age data are from Wagner et al. (1994); lengths from Wagner et al. (1994) and Wauschkuhn et al. (2015; excluding one analyst).

In contrast, the calculated length profile does not fit the measured lengths (Wagner et al., 1994; Coyle et al., 1997; Wauschkuhn et al., 2015). This could mean that the annealing model is inappropriate or inaccurate, but there are also possible experimental factors. Not all measurements were done on prism faces and the tracks were measured by different analysts using different protocols. Figure 9b excludes data from an inexperienced person using a weak etch, which are offset to lower values from the remaining data (Ketcham, 2019; Figure 3.5). Shorter measured lengths can be due to the selection and measurement of the confined tracks (Ketcham et al., 2015; Jonckheere, 2023). The remaining mean lengths are constant down to 1.5 km depth, whereas the calculated profile predicts a ¾-µm decrease. The measured lengths down to this depth (~50 °C) are however within ¼ µm of the values predicted for ambient temperature annealing. Even an approximate fit, coupled with the lack of variation, could indicate that ambient-temperature annealing at lab and geological timescales are connected, and distinct from high-temperature annealing. The mean length data are at present far from conclusive, and a detailed reinvestigation is in progress.

6. Conclusion

This contribution discusses a different take on the apatite annealing data of Carlson et al. (1999), Barbarand et al. (2003), Ravenhurst et al. (2003), and Tamer and Ketcham (2020). Our approach

https://doi.org/10.5194/egusphere-2026-1924
Preprint. Discussion started: 14 April 2026

is a step back compared to earlier studies, in that it is limited to the mean track length, and thus ignores the orientations of individual tracks. We distinguish three annealing phenomena which were hitherto captured in one equation: (1) gradual shortening and (2) accelerated shortening at high temperature, and (3) ambient-temperature annealing. Following Carlson (1990), our model is formulated in terms of the absolute ($S = L_0 - L$) instead of the relative ($r = L/L_0$) length reduction. The reasons are that (1) the unannealed mean length (L_0) in different apatites is correlated with their etch rate (*Dpar*), and so not with the latent track properties (Carlson et al., 1999), (2) fission tracks in different apatites undergo the same absolute shortening (S) under the same annealing conditions up to the point of accelerated annealing (Figures 1 and S1), and (3) the onset of accelerated annealing occurs at different mean lengths in different apatites. One equation gives the mean length reduction up to S ≳2 µm shortening in the least resistant apatite (Renfrew), up to S ≳3 µm in Durango, and up to complete annealing in the most resistant apatite (S ≳8 µm; Bamble). Fitting 489 mean lengths from three different studies leads us to a fanning Arrhenius model with just three parameters, without a transformation of the dependent variable. A linear equation corrects for accelerated shortening of the least resistant apatite compared to the most resistant.

The fit to lab annealing data is in two instances imperfect. One: the model predicts no annealing on lab timescales at ambient temperature, in contrast with experimental data (Donelick et al., 1990; Tamer and Ketcham, 2020). Two: the residuals for the unannealed reference samples are negative, with values up to -1 µm (Supplement Table T2; A_2 = -0.99 µm). This, at first sight, implies that the annealing model is incorrect. On the other hand, it could be the result of fitting a rigid model that is so well constrained over the remainder of data range that it reveals an offset due to a different mechanism than that responsible for the higher-temperature results, e.g., due to ambient-temperature annealing. This is speculative, but it relates both mismatches to a common cause, one that can also account for the extent of ambient-temperature annealing in geological samples. If it is indeed the case, it indicates that the "etchable" mean length of tracks held at absolute zero temperature for any length of time is ~1 µm longer than that of the unannealed induced tracks, in fair agreement with the estimates of Tamer and Ketcham (2020; 0.74 to 1.49 µm) and with the estimated initial length of fluorapatite sample B-5 of Laslett and Galbraith (1996).

The fit to geological data is ambiguous. The age profile for the KTB fits the measurements almost without compromise. This positive result should not be overrated: the calculations assume that the tracks annealed in accordance with the apatites' Cl-contents, and not their OH-contents. The fit also depends on other factors, in particular the assumed cooling histories. However, the thermochronological and independent geological constraints are at least as good as for other reference samples (Wauschkuhn et al., 2015; Figure 8). In contrast, the calculated mean-length profile does not fit the data at all well, but overestimates the measured values over the entire 4 km depth of the pilot hole. There are however experimental factors related to etching, selection and measurement of confined tracks that could be responsible for the mismatch. Measurements on ion-irradiated samples with full control of the track orientations and effective etch times are in progress.

There appears to be no simple equation that provides a natural fit to both lab and geological track length data. From the perspective of statistical leverage, geological data far outweigh lab data for the purpose of fitting annealing equations used for modelling geological thermal histories, to the extent that lab annealing data are almost irrelevant (Guedes et al., 2008). On the other hand, geological reference samples cover a much more limited set of time- and temperature conditions, and their usefulness depends on reliable constraints on their thermal histories. It is moreover important to make sure that the confined track lengths in geological samples are not underestimated due to ambient-temperature annealing or to experimental factors related to their measurement.

https://doi.org/10.5194/egusphere-2026-1924
Preprint. Discussion started: 14 April 2026

Acknowledgements

We acknowledge our debt to the scientists who produced and published the data fundamental to our work.

Funding

Research supported by the German Science Foundation (Deutsche Forschungsgemeinschaft grant JO 356/1).

Author contributions

Concept, funding acquisition, and administration: RJ, TN; formal analysis and validation: RJ, FT, BH; original draft, review and editing: RJ, FT, BH, TN.

Code/data availability

Data are from cited sources; no new data are included.

Competing interests

None

References

Afra B., Lang M., Bierschenk T., Rodriguez M.D., Weber W.J., Trautmann C., Ewing R.C., Kirby N., Kluth P. (2014) Annealing behaviour of ion tracks in olivine, apatite and britholite. Nuclear Instruments and Methods B 326, 126-130.

Aslanian C., Jonckheere R., Wauschkuhn B., Ratschbacher L. (2021) A quantitative description of fission-track etching in apatite. American Mineralogist 106, 518-526.

Aslanian C., Jonckheere R., Wauschkuhn B., Ratschbacher L. (2022) Short communication: Experimental factors affecting fission-track counts in apatite. Geochronology 4, 109-119.

Barbarand J., Carter A., Wood I., Hurford T. (2003) Compositional and structural control of fission-track annealing in apatite. Chemical Geology 198, 107-137.

Carlson W.D. (1990) Mechanisms and kinetics of apatite fission-track annealing. American Mineralogist 75, 1120-1139.

Carlson W.D., Donelick R.A, Ketcham R.A. (1999) Variability of apatite fission-track annealing kinetics. I. Experimental results. American Mineralogist 84, 1213-1223.

Clauser C., Giese P., Huenges E., Kohl T., Lehmann H., Rybach L., Šafanda J., Wilhelm H., Windloff K., Zoth G. (1997) The thermal regime of the crystalline continental crust: implications from the KTB. Journal of Geophysical Research. Solid Earth 102, 18417-18441.

Coyle D. A., Wagner G.A. (1998) Positioning the titanite fission-track partial annealing zone. Chemical Geology 149, 117-125.

Coyle D.A., Wagner G.A., Hejl E., Brown R., Van den haute P. (1997) The Cretaceous and younger thermal history of the KTB site (Germany): apatite fission-track data from the Vorbohrung. Geologische Rundschau 86, 203-209.

Crowley K.D., Cameron M., Schaeffer L. (1991) Experimental studies on annealing of etched fission tracks in fluorapatite. Geochimica et Cosmochimica Acta 55, 1449-1465.

Donelick R.A. (1991) Crystallographic orientation dependence of mean etchable fission track length in apatite: an empirical model and experimental observations. American Mineralogist 76, 83-91.

Donelick R.A., Ketcham R.A., Carlson W.D. (1999) Variability of apatite fission-track annealing kinetics; II, Crystallographic orientation effects. American Mineralogist 84, 1224-1234.

Donelick R.A., Roden M.K., Mooers J.D., Carpenters B.S., Miller D.S. (1990) Etchable length reduction of induced fission

https://doi.org/10.5194/egusphere-2026-1924
Preprint. Discussion started: 14 April 2026

tracks in apatite at room temperature (~23°C): crystallographic orientation effects and "initial" mean lengths. Nuclear Tracks and Radiation Measurements 17, 261-265.

Durrani S., Bull R. (1987) Solid state nuclear track detection: principles, methods and applications. Pergamon Press, Oxford, pp. 304.

Fu Hongyang, Trilsch F., Jonckheere R., Ratschbacher L. (2024) Compositional effects on the etching of fossil confined fission tracks in apatite. American Mineralogist 109, 2026-2036.

Galbraith R.F. (1981) On Statistical Models for Fission Track Counts. Mathematical Geology 13, 471-478.

Gleadow A.J.W., Duddy I.R. (1981) A natural long-term track annealing experiment for apatite. Nuclear Tracks 5, 169-174.

Gleadow A.J.W., Duddy I.R., Lovering J.F. (1983) Fission track analysis: a new tool for the evaluation of thermal histories and hydrocarbon potential. Australian Petroleum Exploration Association Journal 23, 93-102.

Green P.F. (1988) The relationship between track shortening and fission track age reduction in apatite: combined influences of inherent instability, annealing anisotropy, length bias and system calibration. Earth and Planetary Science Letters 89, 335-352.

Green P.F., Duddy I.R., Gleadow A.J.W., Tingate P.R., Laslett G.M. (1985) Fission-track annealing in apatite: track length measurements and the form of the Arrhenius plot. Nuclear Tracks 10, 323-328.

Green P.F., Duddy I.R., Gleadow A.J.W., Tingate P.R., Laslett G.M. (1986) Thermal annealing of fission tracks in apatite 1. A qualitative description. Chemical Geology (Isotope Geoscience Section) 59, 237-253.

Guedes S., Hadler Neto J.C., Iunes P.J., Tello Saenz C.A. (2004) Kinetic model for the relationship between confined fission-track length shortening and fission-track age reduction in minerals. Nuclear Instruments and Methods B217, 627-636.

Guedes S., Jonckheere R., Moreira P.A.F.P., Hielscher R. (2008) On the calibration of fission-track annealing models. Chemical Geology 248, 1-13.

Hendriks B.W.H., Redfield T.F. (2005) Apatite fission track and (U-Th)/He data from Fennoscandia: an example of underestimation of fission track annealing in apatite. Earth and Planetary Science Letters 23, 443-458.

Jonckheere R. (2023) On etching, selection and measurement of confined fission tracks in apatite. Geo-chronology Discussions [preprint], https://doi.org/10.5194/gchron-2023-13.

Jonckheere R., Van den haute P. (1998) On the frequency distributions per unit area of the dimensions of fission tracks revealed in an internal and external mineral surface and in the surface of an external detector. Radiation Measurements 29, 135-143.

Jonckheere R., Van den haute P. (1999) On the frequency distributions per unit area of the projected and etchable lengths of surface-intersecting fission tracks: influences of track revelation, observation and measurement. Radiation Measurements 30, 155-179.

Jonckheere R., Van den haute P. (2002) On the efficiency of fission-track counts in an internal and external apatite surface and in a muscovite external detector. Radiation Measurements 35, 29-40.

Ketcham R.A., Donelick R.A., Balestrieri M.L., Zattin M. (2009) Reproducibility of apatite fission-track length data and thermal history reconstruction. Earth and Planetary Science Letters 284, 504-515.

Ketcham R.A. (2019) Fission-track annealing: From geologic observations to thermal history modeling. In: M.G. Malusà and P.G. Fitzgerald (eds.), Fission-Track Thermochronology and its Application to Geology, Springer Textbooks in Earth Sciences, Geography and Environment, 49-75.

Ketcham R.A., Carter A., Donelick R.A., Barbarand J., Hurford A.J. (2007) Improved modelling of fission-track annealing in apatite. American Mineralogist 92, 799-810.

Ketcham R.A., Carter A., Hurford A.J. (2015) Inter-laboratory comparison of fission-track confined length and etch figure measurements in apatite. American Mineralogist 100, 1452-1468.

Ketcham R.A., Donelick R.A., Carlson W.D. (1999). Variability of fission-track annealing kinetics. III. Extrapolation to geological time scales. American Mineralogist 84, 1235–1255

Laslett G.M., Galbraith R.F. (1996) Statistical modelling of thermal annealing of fission tracks in apatite. Geochimica et Cosmochimica Acta 60, 5117-5131.

https://doi.org/10.5194/egusphere-2026-1924
Preprint. Discussion started: 14 April 2026

Laslett G.M., Green P.F., Duddy I.R., Gleadow A.J.W. (1987) Thermal annealing of fission tracks in apatite 2. A Quantitative Analysis. Chemical Geology (Isotope Geoscience Section) 65, 1-13.

Li W., Kluth P., Schauries D., Rodriguez M.D., Lang M., Zhang F., Zdorovets M., Trautmann C., Ewing R.C. (2014) Effect of orientation on ion track formation in apatite and zircon. American Mineralogist 99, 1127-1132.

Li W., Lang M., Gleadow A.J.W., Zdorovets M.V., Ewing R.C. (2012) Thermal annealing of unetched fission tracks in apatite. Earth and Planetary Science Letters 321-322, 121-127.

Li W., Shen Y., Zhou Y., Nan S., Che C.-H., Ewing R.C. (2017) In situ TEM observation of alpha particle induced annealing of radiation damage in Durango apatite. Nature Scientific Reports 7, 14108 (1-10).

McDannell K.T., Issler D.R., O'Sullivan P.B. (2019) Radiation-enhanced fission track annealing revisited and consequences for apatite thermochronometry. Geochimica et Cosmochimica Acta 252, 213-239.

Nadzri A., Schauries D., Mota-Santiago P., Muradoglu S., Trautmann C., Gleadow A.J.W., Hawley A., Kluth P. (2016) Composition dependent thermal annealing behaviour of ion tracks in apatite. Nuclear Instruments and Methods B 379, 211-214.

Nadzri A., Schauries D., Mota-Santiago P., Trautmann C., Gleadow A.J.W., Hawley A., Kluth P. (2017) Composition and orientation dependent annealing of ion tracks in apatite - Implications for fission track thermochronology. Chemical Geology 451, 9-16.

Paul T.A. (1993) Transmission electron microscopy investigation of unetched fission tracks in fluorapatite - physical process of annealing. Nuclear Tracks and Radiation Measurements 21, 507-511.

Paul T.A., Fitzgerald P.G. (1992) Transmission electron microscopic investigation of fission tracks in fluorapatite. American Mineralogist 77, 336-344.

Ravenhurst C.E., Roden-Tice M.K., Miller D.S. (2003) Thermal annealing of fission tracks in fluorapatite, chlorapatite, manganoanapatite, and Durango apatite: experimental results. Canadian Journal of Earth Science 40, 995-1007.

Spiegel C., Kohn B., Raza A., Rainer T., Gleadow A.J.W. (2007) The effect of long-term low-temperature exposure on apatite fission track stability: a natural annealing experiment in the deep ocean. Geochimica et Cosmochimica Acta 71, 4512-4537.

Stockli D.F., Farley K.A. (2004) Empirical constraints on the titanite (U–Th)/He partial retention zone from the KTB drill hole. Chemical Geology 207, 223-236.

Tamer M.T., Chung L., Ketcham R.A., Gleadow A.J.W. (2019) Analyst and etching protocol effects on the reproducibility of apatite confined fission-track length measurement, and ambient-temperature annealing at decadal timescales. American Mineralogist 104, 1421-1435.

Tamer M.T., Ketcham R.A. (2020) Is low-temperature fission-track annealing in apatite a thermally controlled process? Geochemistry, Geophysics, Geosystems, 21, e2019GC008877 (1-17).

Tello C.A., Palissari R., Hadler J.C., Iunes P.J., Guedes S., Curvo E.A.C., Paulo S.R. (2006) Annealing experiments on induced fission tracks in apatite: Measurements of horizontal-confined track lengths and track densities in basal sections and randomly oriented grains. American Mineralogist 91, 252-260.

Trilsch F., Fu Hongyang, Jonckheere R., Ratschbacher L. (2023) Effective etch times of fossil fission tracks in geological apatite samples and impact on temperature-time modelling. Lithosphere 2023, Number Special 14, Article ID lithosphere_2023_339, 17.

Vrolijk, P., Donelick, R.A., Queng, J., Cloos, M. (1992) Testing models of fission track annealing in apatite in a simple thermal setting: site 800, leg 129. In Larson R.L., Lancelot Y. (eds.), Proceedings of the Ocean Drilling Program, Scientific Results 129, 169–176.

Wagner G.A., Hejl E., Van den haute P. (1994) The KTB fission-track project: methodical aspects and geological implications. Radiation Measurements 23, 95-101.

Warnock A.C., Zeitler P.K., Wolf R.A., Bergman S.C. (1997) An evaluation of low-temperature apatite U–Th/He thermochronometry. Geochimica et Cosmochimica Acta 61, 5371-5377.

Wauschkuhn B., Jonckheere R., Ratschbacher L. (2015) The KTB apatite fission-track profiles: building on a firm foundation? Geochimica et Cosmochimica Acta 167, 27-62.

Wolfe M.R., Stockli D.F. (2010) Zircon (U–Th)/He thermochronometry in the KTB drill hole, Germany, and its implications for bulk He diffusion kinetics in zircon. Earth and Planetary Science Letters 295, 69-82.